Geochemistry Geophysics Geosystems G3

Article
Volume 12, Number 7
28 July 2011
Q0AG05, doi:10.1029/2011GC003666
ISSN: 1525-2027

Published by AGU and the Geochemical Society

The 3-D geometry of detachment faulting at mid-ocean ridges

T. J. Reston
School of Geography, Earth and Environmental Sciences, University of Birmingham, ES 117, Edgbaston, Birmingham B15 2TT, UK (t.j.reston@bham.ac.uk)

C. R. Ranero
Barcelona Center for Subsurface Imaging, ICREA, Instituto de Ciencias del Mar, CSIC, Pg. Marítim de la Barceloneta 37-49, E-08003 Barcelona, Spain

[1] Seismic images of Cretaceous slow spreading crust from the eastern Central Atlantic provide new constraints on the process of seafloor spreading and the importance of detachment faulting. The seismic depth sections image detachment faults that appear to have exhumed footwall massifs of similar geometry to massifs of plutonic and mantle rocks mapped at the present Mid-Atlantic Ridge. The detachments are consistent with the structure and microearthquakes of the Mid-Atlantic Ridge at 26°N, with the footwall rotation inferred from paleomagnetic data and with numerical modeling of oceanic detachments. Other seismically imaged detachments have similar dimensions and geometry, but are covered by a layer of small fault blocks. The detachment types differ in whether or not the fault locks up in the subsurface, probably controlled by the fault strength, the elastic thickness, and whether the exhumed footwall is partly covered by basalts. Toward the segment middle, decreasing mantle serpentinization, decreasing elastic thickness, and thicker median valley basalts all increase the likelihood that the fault locks up, and a new fault propagates upwards from the still active root zone, transferring a slice of the hanging wall to the footwall, to be rafted with the footwall out of the median valley. As a result an oceanic detachment fault, exhuming the footwall at a segment end to form an oceanic core complex, may disappear laterally beneath rafted blocks; detachment faulting may be more widespread at slow spreading ridges than interpreted from seafloor mapping.

Components: 10,000 words, 14 figures.

Keywords: detachment fault.

Index Terms: 3035 Marine Geology and Geophysics: Midocean ridge processes; 3045 Marine Geology and Geophysics: Seafloor morphology, geology, and geophysics; 8178 Tectonophysics: Tectonics and magmatism.

Received 18 April 2011; **Revised** 27 April 2011; **Accepted** 28 April 2011; **Published** 28 July 2011.

Reston, T. J., and C. R. Ranero (2011), The 3-D geometry of detachment faulting at mid-ocean ridges, *Geochem. Geophys. Geosyst.*, *12*, Q0AG05, doi:10.1029/2011GC003666.

Theme: Oceanic Detachment Faults
Guest Editors: J. P. Canales, M. Cheadle, J. Escartin, G. Fruh-Green, and B. John

1. Introduction

[2] At slow spreading ridges, large offset normal faults, termed oceanic detachment faults, thin the crust to form asymmetric mid-ocean ridge (MOR) structures. An oceanic detachment fault is typically located on one MOR flank where it exhumes plutonic lower crust and mantle rocks, which form a

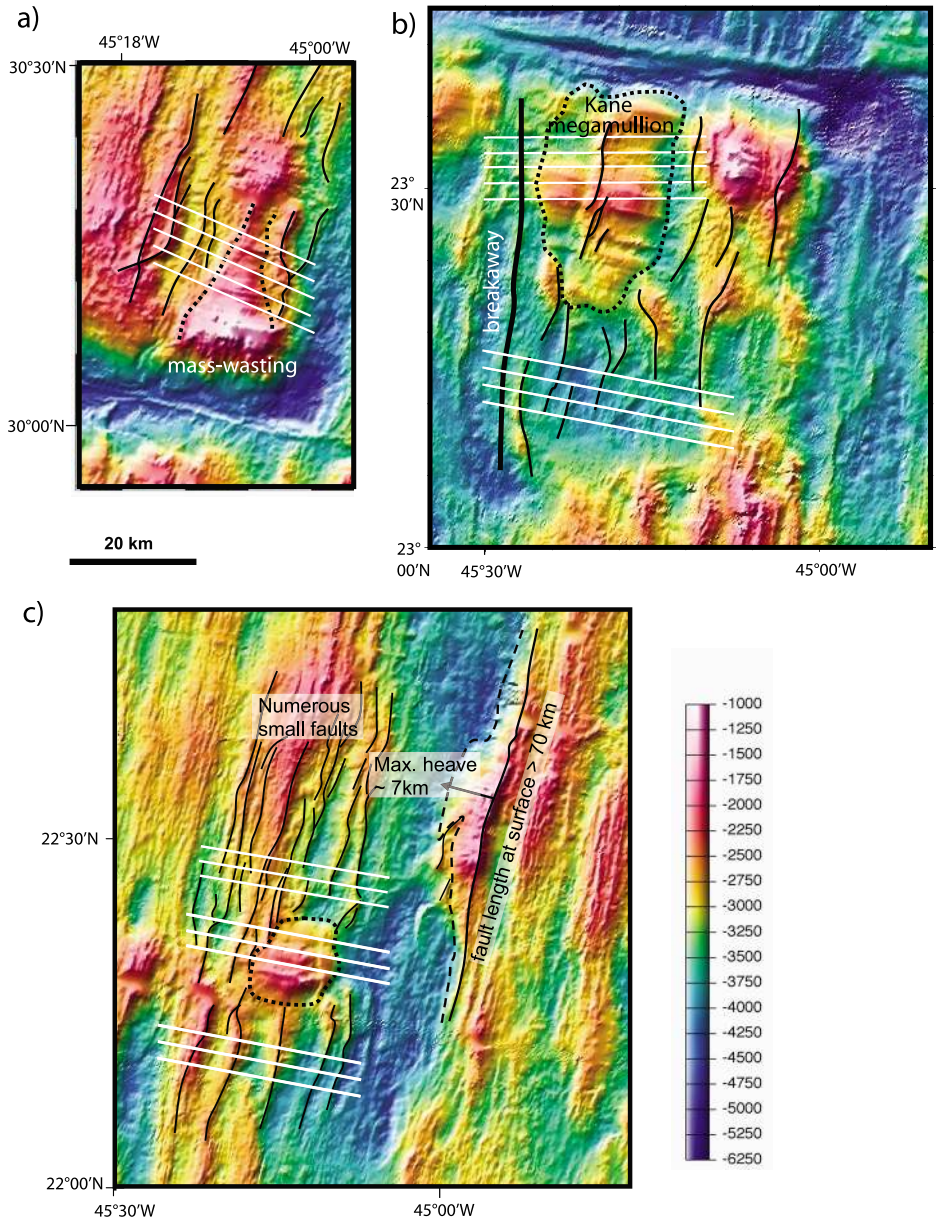

Figure 1. Shaded relief bathymetry of three oceanic core complexes. Broken lines outline corrugated surfaces; thin black lines are faults. (a) Atlantis Massif just north of the Atlantis transform, showing corrugated surface narrowing northward. (b) South Kane Inside Corner. The Kane Megamullion is semioval, elongated by a factor of just under 2 in the isochron (strike) direction, dying out laterally in an area of reduced topography marked by small faults. This may be a transfer zone of some sort. (c) Roughly circular OCC at 22°15 N [*Dannowski et al.*, 2010] is replaced to the north and south by faults spaced 2–5 km apart with a maximum peak-trough topography of ~500 m. Note developing large-offset fault on eastern flank of the median valley: this may be an incipient OCC. White lines show locations of bathymetric profiles shown in Figures 8, 9, and 10.

domal massif, termed an oceanic core complex (OCC) by analogy with metamorphic core complexes [*Cann et al.*, 1997; *Tucholke et al.*, 1998; *Dick et al.*, 2008; *Dannowski et al.* 2010]. The upper surface of the massif is commonly marked by a series of spreading parallel striations and corrugations (Figure 1), thought to indicate the transport direction of the hanging wall relative to the footwall [*Cann et al.*, 1997; *Tucholke et al.*, 1998; *Blackman et al.*, 1998].

[3] Detailed microstructural studies coupled with the observation of corrugations at a variety of scales [*MacLeod et al.*, 2002; *Escartín et al.*, 2003]

show that the corrugated and striated surfaces are the slip surface of large-offset brittle faults that cut to depth beneath the median valley. Palaeomagnetic studies have shown that the faults were active at moderate to steep angles (45°–60°) and were rotated to their current low-angle orientation [*Garcés and Gee*, 2007; *Morris et al.*, 2009]. This geometry is consistent with a rolling hinge model in which a steep fault rotates to low angle as the footwall is flexurally unloaded [*Morris et al.*, 2009].

[4] Although the dimensions of the corrugated surfaces demonstrate the importance of very large offset normal faults at the end of the spreading segments, tectonic extension toward the middle of the segments is generally thought to be accommodated along steep, comparatively small offset, normal faults [*Shaw and Lin*, 1993]. However, it is not clear how the transition from an oceanic detachment to such an array of smaller faults can occur without leading to strain compatibility problems. In this paper we propose that detachment faults observed as corrugated surfaces at the ends of segments may extend laterally toward the middle of the segments where they are overlain by small fault blocks that are part of the same fault system. In particular, we explore the possibility below that OCCs are simply those places where a laterally more extensive detachment system breaks the surface, elsewhere the detachment being covered by a series of fault blocks.

2. Seismic Images of Cretaceous Oceanic Detachments

[5] Most work on faulting at MORs has been based on seafloor mapping near the spreading center where the tectonic structure of the igneous crust can be imaged before it is obscured by sedimentary blanketing, but seafloor mapping does not provide information on the structure at depth. This third dimension can be constrained by seismic data, but apart from a survey reported by *Canales et al.* [2004] (discussed more below), there are few reported seismic images of faulting associated with OCCs at present-day slow spreading ridges, in part due to imaging problems caused by severe scattering of the seismic waves at the seafloor of unsedimented areas at MORs. However, ancient seafloor has been blanketed by sediments, reducing the scattering and hence imaging problems, providing clearer images of ancient oceanic crust that can reveal the geometry of the structures that developed during seafloor spreading.

[6] Most seismic data across oceanic crust have been presented as time sections or depth-stretched profiles, interpreted as showing relatively steeply dipping faults, and interpreted as the deep fault geometry of the common tilted-block MOR seafloor morphology [e.g., *White et al.*, 1994; *Ranero et al.*, 1997a, *Singh et al.*, 2006]. In general, the relationship between the geometry of the deep structure and basement morphology has been little explored, partly because of the difficulty in comparing time sections with depth maps and partly due to the imaging problems prevalent in time sections. Both problems can be reduced by applying prestack depth migration; here we summarize observations made from different surveys over Cretaceous oceanic crust from the eastern Central Atlantic [*Reston et al.*, 1996; *Ranero and Reston*, 1999; *Reston et al.*, 2004a]. These data are all close to flow lines (Figure 2) and have all been prestack depth migrated, providing depth images (Figure 3) of the eastern half of oceanic crust formed at the Mid-Atlantic Ridge over a period of several millions of years in the Cretaceous.

[7] Two types of "detachment fault" have been recognized on these seismic depth images (Figure 4). Convex-up basement highs are bounded on their ridgeward side by reflections that can be traced from the top of the basement into the igneous crust at an angle of 30–45° (Figures 4a and 4b). We interpret these highs as oceanic core complexes (OCCs) representing the exhumed footwalls of oceanic detachment faults that extend into the basement along dipping reflections labeled F6, F7 and F8 (Figures 4a and 4b). We trace the exhumed slip surface along the top of basement until there is a distinct change in the dip of the top of basement, the breakaway. Outboard of the breakaway (footwall basement cutoff), the top of basement has been flexurally rotated to form a narrow basin, as observed behind the breakaway at OCCs mapped near the spreading axis [*Smith et al.*, 2008]. On the ridgeward side of the convex-up highs, we interpret ridgeward dipping reflections to define the faults until they become unclear at depths greater than ~2 km beneath the top of basement. Previous interpretations [*Reston et al.*, 2004a] proposed that the faults may continue at moderately low angles, but it is also possible that at greater depths the faults become too steep (>45°) to be well imaged; a downward steepening of the fault plane is consistent with other geophysical data as discussed below. The continuation of the fault beneath the top of basement emphasizes that describing the line where the fault dives beneath the hanging wall as the

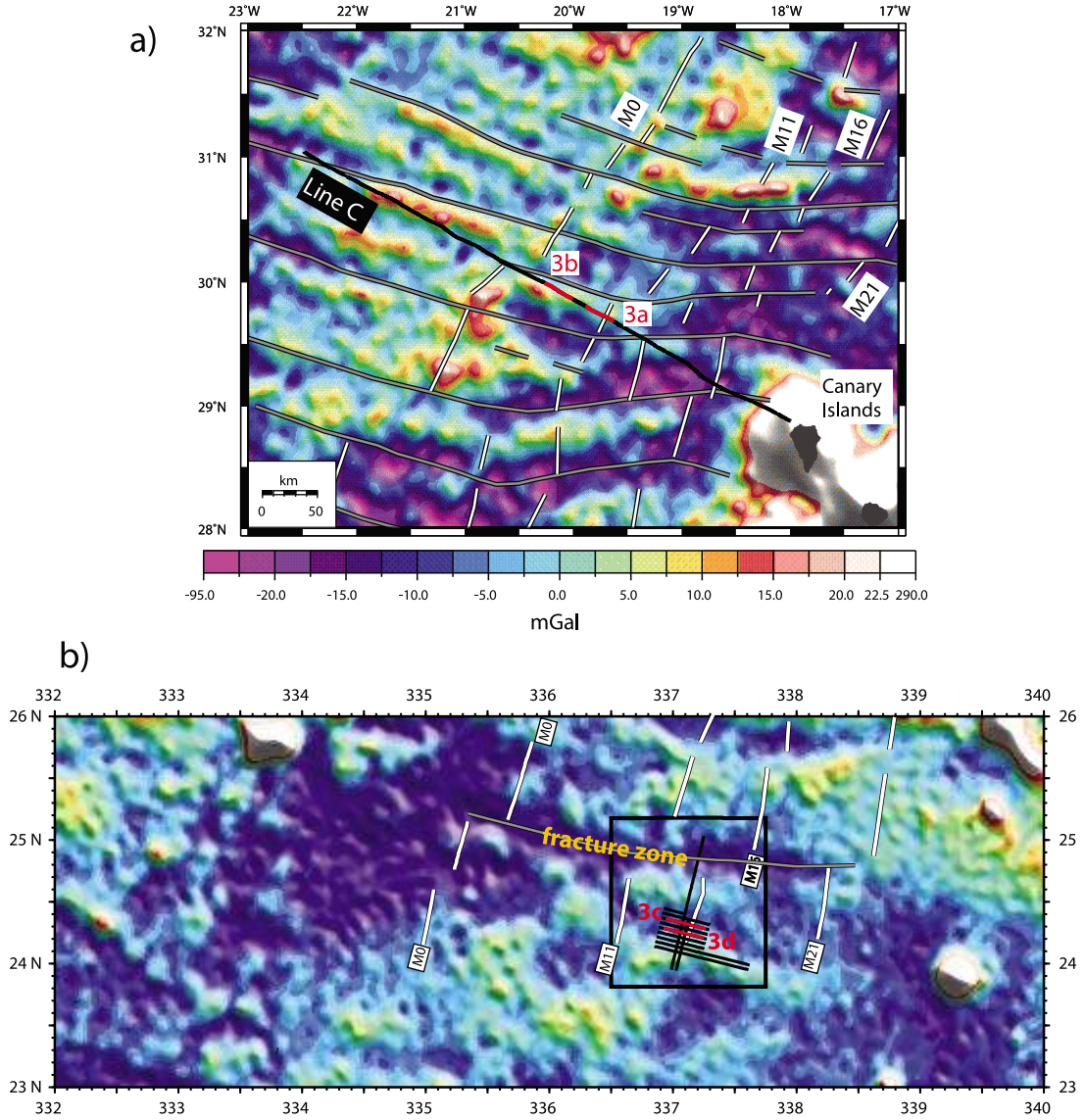

Figure 2. Location of seismic images produced by prestack depth migration shown in red relative to the longer profiles. The portion of Canary line C (Figures 3a and 3b) that images structures F6, F7, and F8 runs just along the inside corner side of a fracture zone, identified in both the gravity [*Smith and Sandwell*, 1995] and in the offset of magnetic anomalies M0-M21 [*Ranero and Reston*, 1999]. Profiles BIRPS OCEAN 5 and 7 lie well to the south of a major fracture zone in a region of subdued gravity (subdued topography).

"termination" [e.g., *Canales et al.*, 2008; *Blackman et al.*, 2009; *MacLeod et al.*, 2009] is very misleading (Chapman Conference, Cyprus, May 2010) and should be dropped in favor of a term such as "top hanging wall cutoff." The traditional map term "fault trace," which is not generally used on sections, is not appropriate as it cannot be used to describe the geometry of a structure everywhere buried by later sedimentary rock.

[8] The structures described above appear to be detachment faults that have controlled the exhumation of the footwall to form a domal massif, in the same way that detachments appear to form OCCs at active spreading centers. However, in the Cape Verde Abyssal Plain and Canary Basin, depth images along flow lines away from the segment ends reveal subhorizontal structures which we interpret as a second type of detachment fault, occurring beneath a series of small fault blocks (Figures 4c, 4d, and 4e) [*Reston et al.*, 1996]. Subhorizontal reflections at similar depths in fast spreading crust have been interpreted as the base of the sheeted dikes or a hydrothermal front, and deeper dipping reflections as magmatic layering, possibly modified by shearing [*Ranero et al.*,

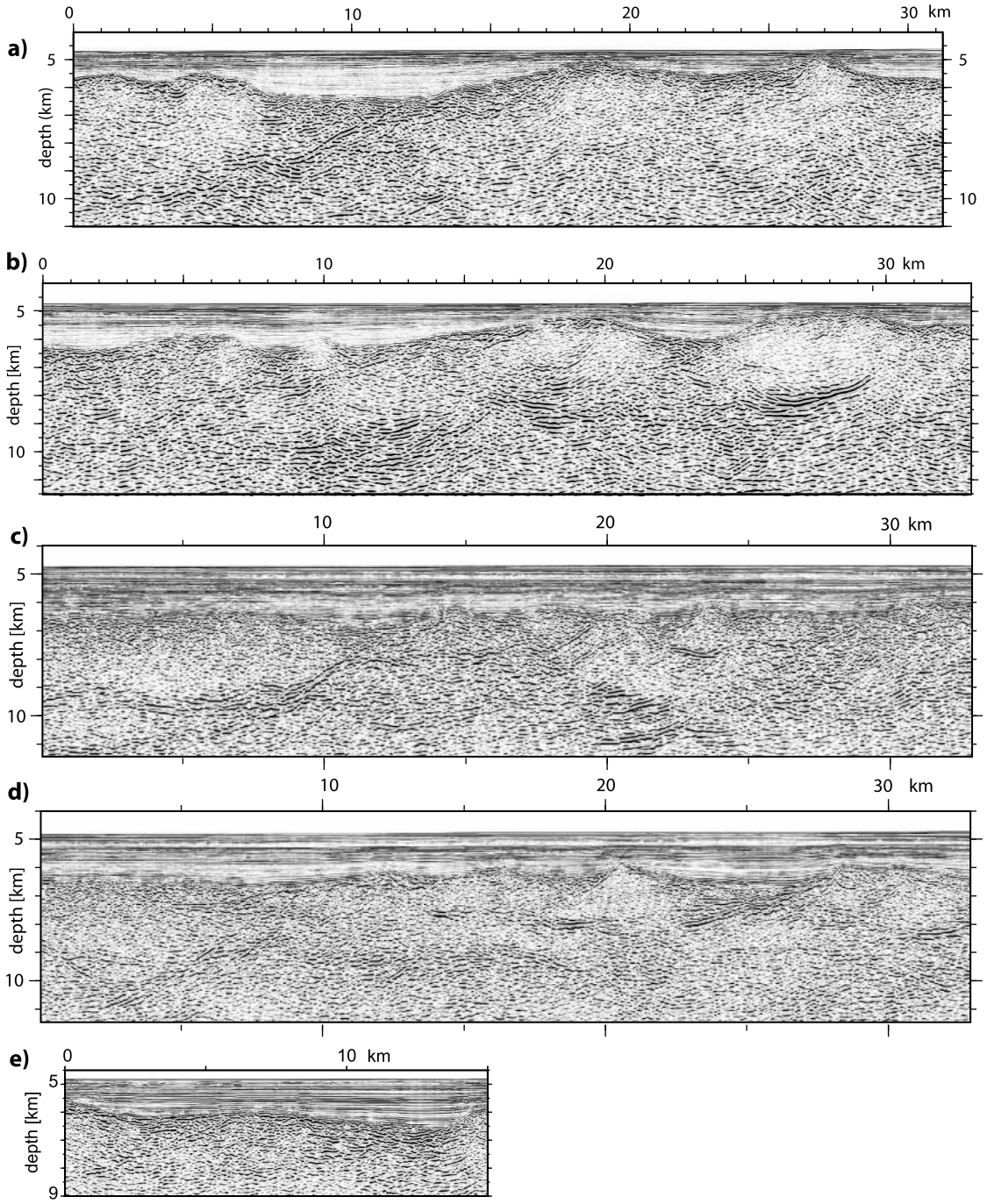

Figure 3. Seismic depth images produced by prestack depth migration. (a, b) Portions of profile Canary C, running along the inside corner of a Cretaceous fracture zone (Figure 2). (c, d) BIRPS OCEAN profiles 5 and 7 and (e) portion of Canary Line B [*Reston et al.*, 2004a], located away from fracture zones. Interpretations of these profiles are shown in Figure 4.

1997b]. However, the subhorizontal structures and their deeper ridgeward dipping continuations imaged beneath the Cape Verde Abyssal Plain are likely to be brittle "detachment faults" [*Reston et al.*, 1996; *Reston et al.*, 2004a] because they can be traced to apparent breakaways away from the ridge, they appear to mark the lower limit of faults bounding the overlying fault blocks, and they are bounded on their younger side by ridgeward dipping reflections consistent with a more steeply

dipping root zone toward the ridge. Furthermore, the geometries of these "detachment systems" (D1, D2, D3; Figures 4d, 4c, and 4e) resemble detachment faults identified at rifted margins [e.g., *Reston*, 1996; *Reston et al.*, 2004b] and, as discussed below, are consistent with *Buck*'s [1988] rolling hinge model for detachment formation in which the faults form a series of fault segments that are sequentially active and then rotated rather than a single fault surface that moved at low angle.

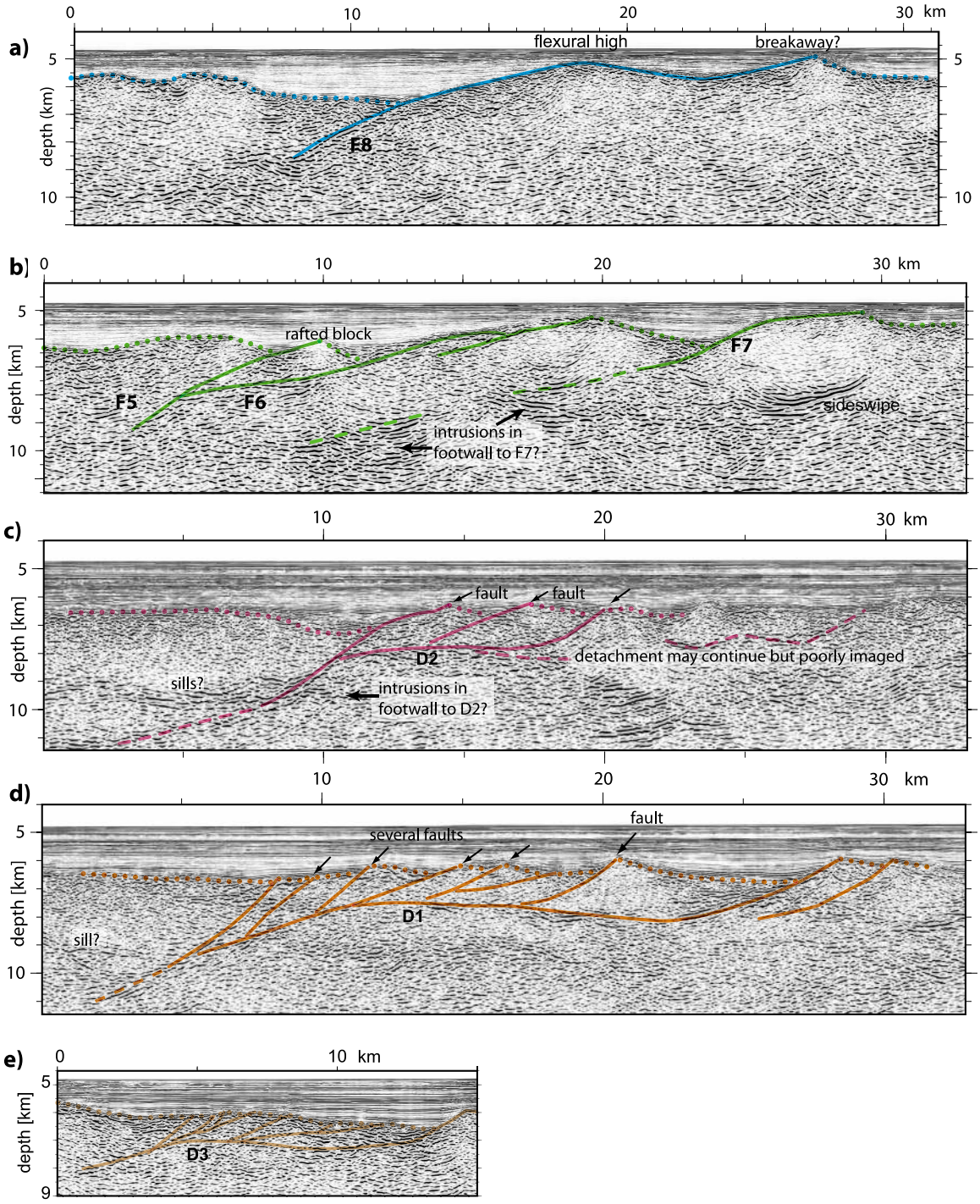

Figure 4

[9] The dimensions of the D1, D2 and D3 detachment faults imaged beneath the fault blocks are similar to that of the F detachments that defines the top of basement for much of their length (Figure 4). Both types of structures cut to 3–5 km depth beneath the top of basement, in the case of D1 and F8 ~20 km ridgeward from a breakaway where they intersected the top of basement, in the case of D2, D3 and F6, F7, about 7–10 km from the breakaway. At and immediately outboard of the breakaway, the footwall cutoff for F8, F7 and the D structures has been back rotated by ~25–30° to form a small basin, consistent as discussed below with the flexure of a normal fault. It is thus likely that the two types of detachment fault have a similar origin. If the F structures are detachments that exposed the top of basement at the seafloor during Cretaceous seafloor spreading, it is possible that the D structures and represent the lateral continuation beneath a series of small fault blocks of similar OCC detachments.

3. Comparison With Model Detachments

[10] The detachment faults interpreted on seismic images can be compared to the geometry predicted by numerical and other models of detachment faults (Figure 5). Such a comparison may test the interpretation of the seismic, provide insight into the interactions between closely spaced detachment faults and the evolution of the detachment systems, provide estimates of the elastic thickness of the lithosphere during detachment formation and constrain the proposed geometry of other detachment faults. We compare (Figures 5a and 5b) the seismic geometry of the F8 detachment (Figure 4a), shortened by a factor of 0.96 to allow for 15° between the profiles and true flow lines, with various published numerical models, from *Lavier et al.* [1999], *Tucholke et al.* [2008], and *Schouten et al.* [2010]; the details of the modeling can be found in those papers. *Schouten et al.*'s [2010] models differ from the others by requiring the detachment to root at an angle ~60°, in keeping with Andersonian fault mechanics, and in agreement with both the distribution of microearthquakes in the TAG area of the Mid-Atlantic Ridge at 26°N [*deMartin et al.*, 2007] (Figure 6) and with the footwall rotation inferred from paleomagnetic studies [*Garcés and Gee*, 2007; *Morris et al.*, 2009].

[11] To better fit the seismic geometry, the modeled geometry has where necessary been scaled to reflect different lithospheric elastic thicknesses (T_e). As the flexural parameter which controls the wavelength of the flexure varies as $T_e^{0.75}$ [*Turcotte and Schubert*, 2002], the geometric scaling factor is the change in elastic thickness T_e to the power of 0.75. Thus if the T_e is reduced by a factor of 2 (scaled by 0.5), the dimensions of the detachment are scaled by a factor of $0.5^{0.75}$, i.e., by ~0.6. In models where T_e is not defined, the direct geometrical scaling factor is given (Figure 5).

[12] Key points of comparison between the models and the seismic images are (1) the dip of the detachment in the subsurface, (2) the frontal slope of the exhumed footwall, (3) the amplitude of the flexural high, (4) the distance of the top hanging wall cutoff (the fault trace when no sediment is present) from the flexural high and from the breakaway, and (5) the amplitude of the breakaway. The model detachments agree reasonably well with the F8 detachment (Figures 4a, 5a, and 5b): the models predict a similar orientation of the detachment in the shallow subsurface, a similar slope of the ridgeward flank of the flexural high, and a similar height of the flexural high and similar shape of the breakaway. The main discrepancy is the wavelength of the flexure and the height of the breakaway: the models predict a longer wavelength flexure and higher breakaway than is observed, suggesting that the elastic thickness of the model lithosphere was greater than that of the newly formed oceanic plate in the Cretaceous, the litho-

Figure 4. Interpretation of profiles shown in Figure 3, showing a variety of detachment faults (solid colored lines) in slow spread oceanic crust from eastern Central Atlantic. Broken lines represent top of basement where this is not an exhumed slip surface. (a, b) Part of Canary Basin line C showing large-offset normal faults. The upper section is reminiscent of a detachment F8 produced by a rolling hinge (top [*Lavier et al.*, 1999]). In both cases, the exhumed slip surface and footwall are interpreted to form large portions of the top of basement. (c, d) BIRPS OCEAN profiles 5 and 7 from the Cape Verde Abyssal Plain, showing subhorizontal to domal reflections beneath the top of basement (D1–D2). As faults appear to detach onto these features, D1 and D2 have been interpreted as detachment faults. Note that their lateral dimension and domal shape are similar to the top of basement faults (F8, F6, F7) shown above. (e) Image from Canary Basin line B, showing a possible detachment fault (D3) poorly imaged beneath a series of small fault blocks. Note similarities with D1 and D2, albeit at a smaller scale. Detachments like this may be present elsewhere but unrecognized on seismic images.

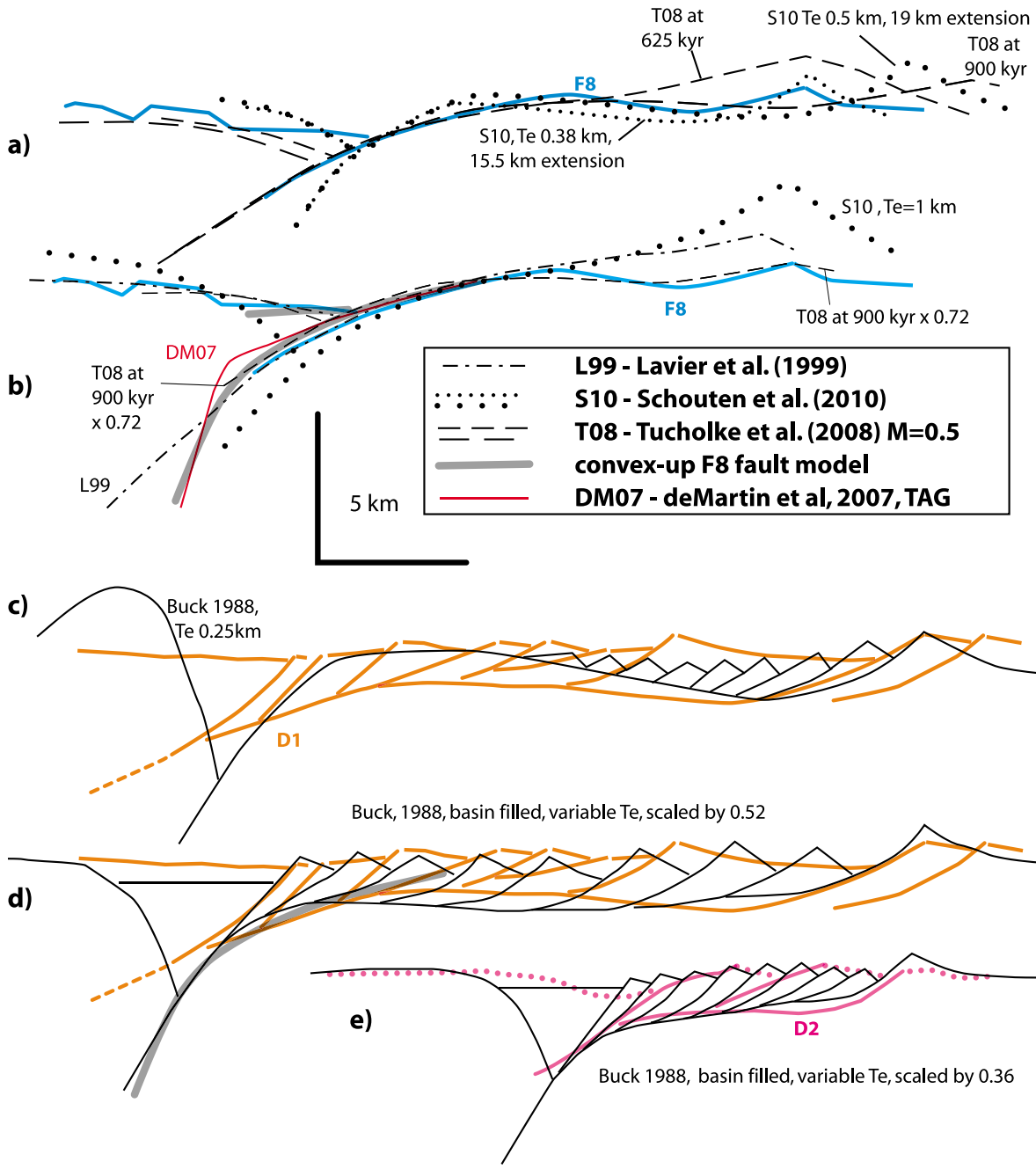

Figure 5. Comparison (without vertical exaggeration) between seismic images of Cretaceous detachment faults and geometries of detachments derived from numerical models. T08 is the detachment of *Tucholke et al.* [2008] produced when magmatism takes up 50% of the plate separation; S10 is from *Schouten et al.* [2010], with elastic thickness (T_e) as given. (a) Comparison between the F8 detachment (corrected for ~15° obliquity to spreading direction) and various models: S10 with T_e of 0.5 km after 19 km extension and T08 after 625 kyr. These do not predict the separate highs of the breakaway and the flexural high and have a breakaway that is too high, implying that both may have too high a T_e; a better fit is obtained by scaling the S10 model for a T_e of 0.38. (b) Comparison between the F8 detachment (corrected for ~15° obliquity to spreading direction) and various models: a good fit is obtained by scaling T08 by a factor of 0.72, i.e., scaling its T_e by 0.64. Thick gray line is simplified curve of frontal portion of F8 extended to depth for comparison with other data. (c) D1 compared to model of *Buck* [1988] with T_e of 0.25 km and no basin fill. The general decrease in size and then absence of rafted blocks in the Buck model does not agree with the D1 observations. (d) Comparison of D1 with *Buck*'s [1988] variable T_e model where the basin is sedimented produces a better fit, implying that the D1 detachment may form where the developing rift is filled with basalt. (e) A similar Buck model can be compared with D2; the main difference is the size of fault blocks.

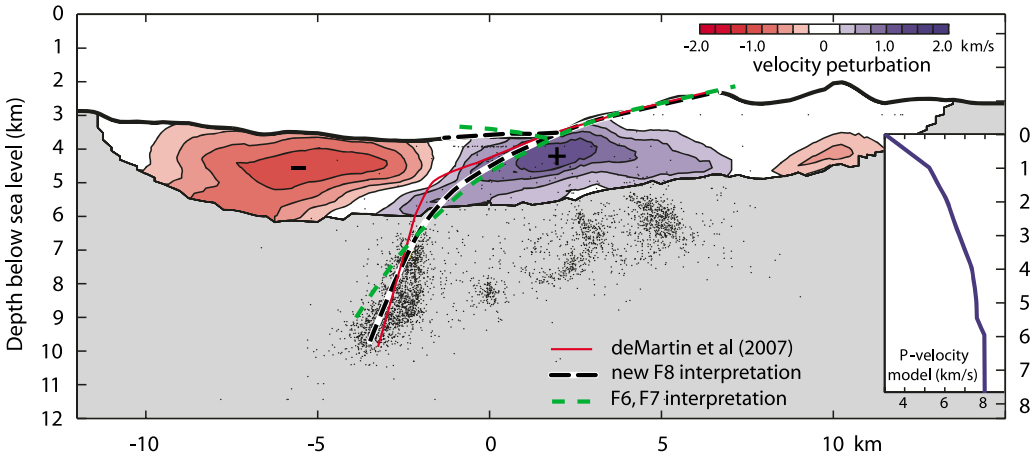

Figure 6. Geophysical constraints on detachment geometry from TAG [*deMartin et al.*, 2007]. Thin red line: existing interpretation [*deMartin et al.*, 2007], consistent [*Blackman et al.*, 2009] with the geometry of F8 [*Ranero and Reston*, 1999]. Modified F8 (dashed black) and F6/F7 (broken green) models presented here fit geometry of exhumed footwall, geometry of high velocity footwall, and distribution of microseismicity at depth at least as well as the deMartin et al. interpretation.

sphere perhaps having been weakened by the initial bending. Reducing T_e improves the fit, but shifts the flexural bulge slightly closer to the hanging wall cutoff compared to the geometry of F8. This might indicate that the elastic thickness is not constant but laterally variable, decreasing as the amount of flexure increases [*Buck*, 1988].

[13] The F8 detachment also dips initially at a lower angle than the models of *Schouten et al.* [2010], but it should be borne in mind that F8 may steepen as its image disappears with depth. Tracing the detachment as far as the image allows and then gradually increasing the curvature until the detachment dips at about 60° produces a convex-up geometry that is consistent with both the seismic and the predictions of fault mechanics. This revised geometry for F8 (Figure 5b), is also consistent with the geophysical data from the TAG area (Figure 6). Here a detachment geometry has previously been constrained by surface geology, seismic velocity structure and microearthquakes [*deMartin et al.*, 2007], and interpreted as two gently curved segments joined by a strongly curved middle segment. *Blackman et al.* [2009] showed that the deMartin et al. interpretation is consistent with the geometry of F8 as interpreted on the seismic [*Ranero and Reston*, 1999], with the upper gently curved segment closely following the best imaged subsurface portion of F8 and its emergent continuation. However, the seismic image used by Blackman et al. had not been corrected for the slight (15°) obliquity of the profile [*Reston et al.*, 2004a]. Following the discussion above, we compare the TAG microearthquakes with the more idealized convex-up fault interpretation of F8 (Figures 5a, 5b, and 6), which does include the obliquity correction. The new detachment geometry matches the microearthquake pattern equally well as the *deMartin et al.* [2007] interpretation while removing the abrupt change in dip and resulting resistance to slip. Furthermore the geometry requires at least 50° of footwall rotation, consistent with the paleomagnetic results of *Garcés and Gee* [2007] and *Morris et al.* [2009].

[14] The published numerical models of oceanic detachments [*Lavier et al.*, 1999; *Buck et al.*, 2005; *Tucholke et al.*, 2008; *Schouten et al.*, 2010; *Olive et al.*, 2010] are all for detachments that are not overlain by a thin layer of tilted fault blocks and as such cannot be directly compared with the D detachments imaged on the British Institutes Reflection Profiling Syndicate's (BIRPS) OCEAN profiles 5 and 7 (Figures 4c and 4d). However, as discussed further below, if the fault locks up in the subsurface, a slice of the hanging wall can be transferred to and rafted with the footwall [*Buck*, 1988]; successive slices cover an inactive, passively rotated "detachment fault." The geometry of such a model, with T_e of 0.25 km matches the overall scale of the D1 detachment (Figure 5c), but unlike D1 has a highly distorted hanging wall and a ridgeward reduction in size of transported fault blocks. Furthermore, the flexural high in the model is greater than the doming of D1 beneath its cover of fault blocks. These differences can be reduced if the valley between the hanging wall and footwall is

continually filled with sediment or, in a ridge setting, with lavas (Figures 5d and 5e), so that the rafted fault blocks are slices of mainly basaltic fill rather than original hanging wall. The main discrepancy between this model and D1 (Figure 5d) is now the dimensions and geometry of the fault blocks above the detachment, and the angle at which the detachment roots. Fewer fault blocks are imaged on the seismic, reflecting either a wider spacing between the formation of new hanging wall fault slices or problems imaging all the faulting. The difference in the angle at which the fault appears to root may be a function of the difficulty in imaging the steep structures, but may also result from a subsequent rotation of the root zone in the footwall to a later fault, as discussed below for F6 and F7. Similar comments apply to the comparison between the model in Figure 5e and the D2 detachment. Interestingly, the two models best matching the seismic geometries in Figures 5d and 5e both have laterally variable T_e, related to the degree of curvature. Similar variations in elastic thickness T_e might improve the already good fit of the constant T_e models [*Schouten et al.*, 2010] to the seismic image of the F8 detachment (Figures 5a and 5b).

[15] The numerical models cannot be directly compared with the geometry of the F7, F6 and F5 detachments as the close spacing of these means that the younger faults have affected the geometry of the older structures through the rotation of the footwall. To illustrate the original geometry of F6 and F7, we show a schematic forward model of the evolution of the F7, F6 and F5 detachments (Figure 7). Initially (Figure 7a), F7 develops, flexes and becomes inactive as continued magmatic spreading moves the root zone away from the ridge axis. A new fault (F6) then develops. Movement along F6 (Figure 7b) is accompanied by the rotation of the footwall to F6, including the root zone to the abandoned F7 detachment. The footwall directly beneath F6 is rotated the most, the rotation decreasing to zero moving away from F6 toward the breakaway of F7. The root zone to F7 is rotated to a dip of ~20°: as rotation increases ridgeward (closer to F6), the F7 fault is straightened from its previous convex-up geometry. Flexure of F6 however coupled with continued magmatism (see below) causes the F6 fault to rotate to an angle at which it can no longer slip, so a steep shortcut fault (F5) propagates up from the root zone of F6 through the hanging wall. Movement on F5 thus rafts a block up and out of the median valley, the block being floored by the now inactive and passively rotating F6 detachment (Figure 7c). This too is rotated to low angle, merging downdip with F5. The result of these three phases of faulting are two convex-up highs faced on the ridgeward side by the exhumed footwall of F7 and F6 both of which continue into the subsurface at low angle, and a rafted block, which together closely resemble the seismic geometry observed on Canary Line C (Figure 7d). The apparent planar (linear in section) low angle subsurface geometry of the F7 and F6 detachments is the result of the flexural rotation of a convex-up fault in the footwall to a similar convex-up fault. The unmodified geometry of these convex-up faults is not dissimilar to F8, and also provides a reasonable fit to the structure and seismicity of the TAG area (Figure 6).

4. Comparison of Basement Topography

[16] Previously we have argued [*Ranero and Reston*, 1999] that the morphology and dimensions of the large F fault structures imaged in the Canary Basin are comparable to those of the seafloor of and around the Atlantis Massif (Figure 8) and the Kane Megamullion (Figure 9a). Here we extend this comparison the 22°12′N OCC (Figure 10) and also compare the bathymetry along strike of the OCC with that above the D detachments.

[17] Three or more parallel bathymetric profiles are taken for each comparison, to demonstrate the consistency of the morphology along strike. The comparison with F6, F7 and F8 are made along bathymetric profiles that are 15° oblique to the flow lines as the Canary C seismic profile is similarly slightly oblique in the region of the F6-F8. However, given the limited lateral extent of the 22°12′N OCC, such an approach would include bathymetry that was not directly ridgeward or directly outboard of the corrugated surface so here we have shortened (to 96%) the length of the seismic structure to correct for the profile obliquity (Figure 10e). The D detachments are imaged on profiles that are flow lines so here the bathymetric profiles used are also along flow lines.

[18] Given the variety of dimensions of OCCs, it is unlikely that all the features of any given OCC can be matched, but key features that are common to most OCCs and also to the numerical models discussed earlier (Figure 5) are the curvature of the ridgeward facing slope of the OCC and the angle at which the slip surface appears to enter the subsurface.

[19] The curvature of the top and the ridgeward facing slope of F8 is similar to those of the Atlantis Massif (Figure 8a; location of bathymetric profiles

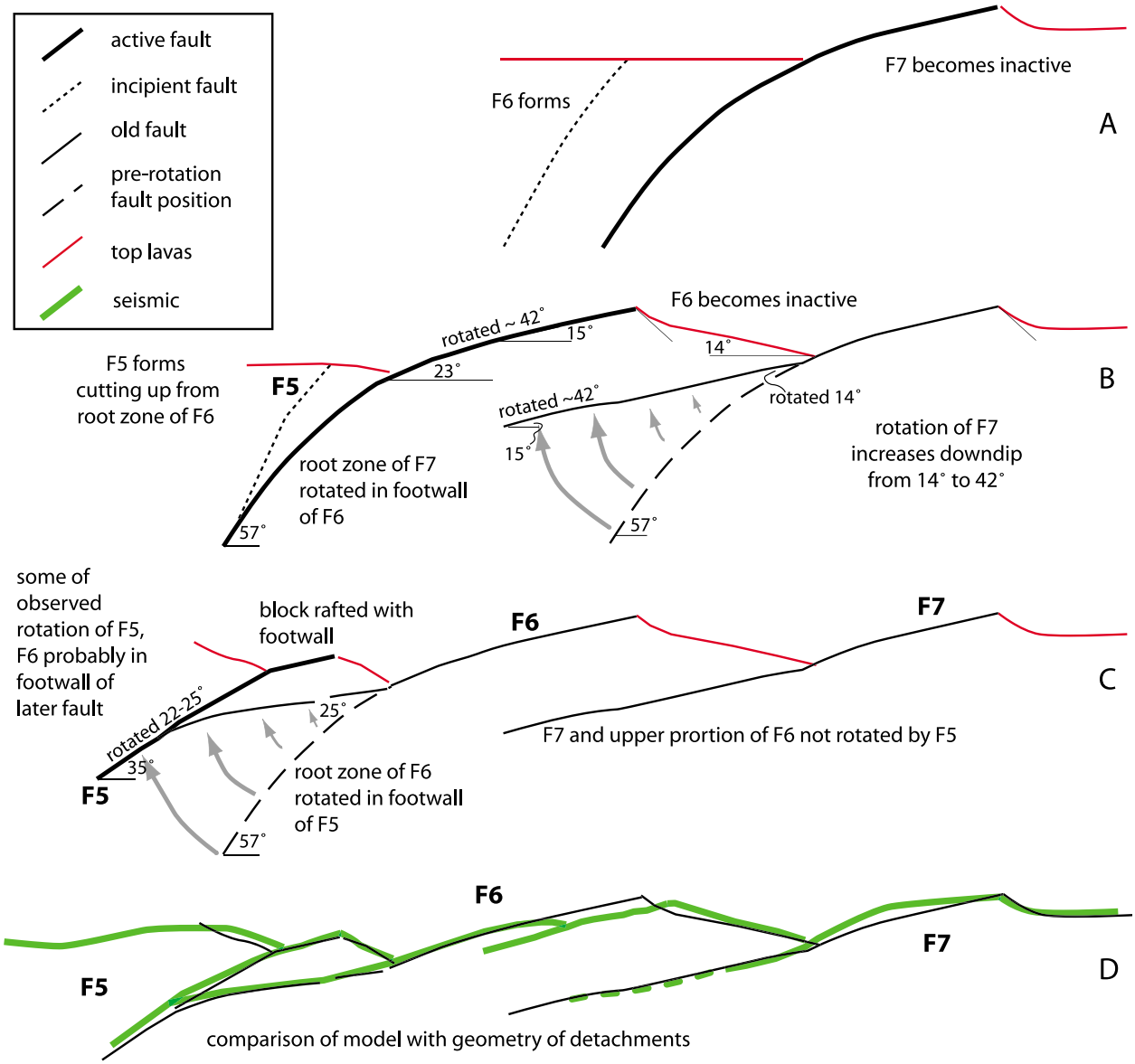

Figure 7. Schematic forward model (no vertical exaggeration) for the development of the F5, F6 and F7 detachments. (a) F7 forms, slips, flexes to a convex-up geometry compatible with the TAG data (Figure 6) and becomes inactive. F6 forms in the hanging wall to F7. (b) Movement along F6 is accompanied by flexure, causing its footwall, including the root zone of F7 to rotate clockwise. As the upper portion of F6 is rotated to <25° within the subsurface, it is abandoned and a new fault (F5) cuts up from its root zone through the hanging wall. (c) Movement along F5 rafts a block up and out of the median valley; the block moves passively with the now inactive F6 detachment. (d) The overall geometry closely resembles that of the seismic (corrected for ~15° obliquity to spreading direction).

shown in Figure 1), although the location of the breakaway differs as the two structures are not identical. Similarly, F6 has a similar frontal slope and footwall height as the Atlantis Massif, and is overlain by a rafted block (bounded by F5) of similar dimension to that on the Atlantis Massif (Figure 8b), but the overall lateral dimension of F6 is smaller as F6 has accommodated far less displacement than the Atlantis Massif detachment. In much the same way, the Kane Megamullion also resembles both F8 and F6 (Figures 9a and 9b) in terms of the curvature of the frontal slope, the angle at which it appears to enter the subsurface (~20°), but not in terms of the overall dimensions of the OCC as the Kane Megamullion has accommodated much more slip.

[20] The core complex at 22°12′N does however have similar dimensions to F8, allowing a fuller comparison (Figure 10e). Although the geometry of the flexure is not the same, particularly between

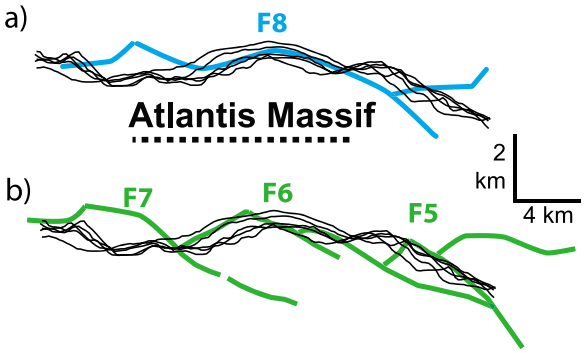

Figure 8. Comparison between the bathymetry over the Atlantis Massif and the topography and fault geometry of the F5, F6, and F8 detachments (Figures 4a and 4b). The basement morphology of the F8 detachment matches the curvature and geometry of the Massif's frontal slope as far as the top of the domal massif reasonably well, and the shape of the breakaway, if not its distance from the hanging wall cutoff. F6 and F5 together match the curvature and geometry of the frontal slope and of the captured rider block, if not the precise position of that block on the underlying detachment.

the flexural high and the breakaway, F8 again closely resembles the 22°12N OCC in terms of the curvature of the frontal slope, the angle at which the detachment enters the subsurface, the overall height of the OCC and its overall wavelength.

[21] These comparisons strengthen our suggestion that F8 is a fully fledged OCC and that F6 (and the neighboring F7) were incipient OCCs before faulting migrated further oceanward (Figure 7).

[22] It is less obvious how to compare the D detachments (Figures 4c, 4d, and 4e) to near ridge structures, as the D detachment are themselves beneath a series of rider blocks. However, one possibility to be explored is that the OCCs are simply places where more extensive detachment systems breaks the surface, and that the lateral continuation of the OCC detachment may be covered in small rider blocks as are the D detachments. We thus compare the basement topography above the D detachments with that along strike of the OCCs, to test the hypothesis that the D detachments may be the along strike equivalent of OCC detachments. Such a comparison cannot prove that the OCC detachments continue laterally in the subsurface, but it does serve to illustrate that possibility.

[23] The Kane Megamullion disappears southwards and is replaced by a more subdued topography of low-amplitude fault blocks. If the detachment were to continue beneath these blocks, its lateral extent would be from the southern continuation of the breakaway to the southern continuation of the ridgeward limit of the corrugated surface in the east. These dimensions (Figure 9c) agree reasonably well with the overall dimension of D1: detachments of this scale may exist beneath an array of small fault blocks. The overall morphology of the top of basement above D1 resembles that along strike of the Kane Megamullion, apart from one pronounced fault scarp above D1. The match with the more regular spaced faulting above D2 is less good, but the eastern portion of the seafloor south of the megamullion closely resembles that above the D3 detachments.

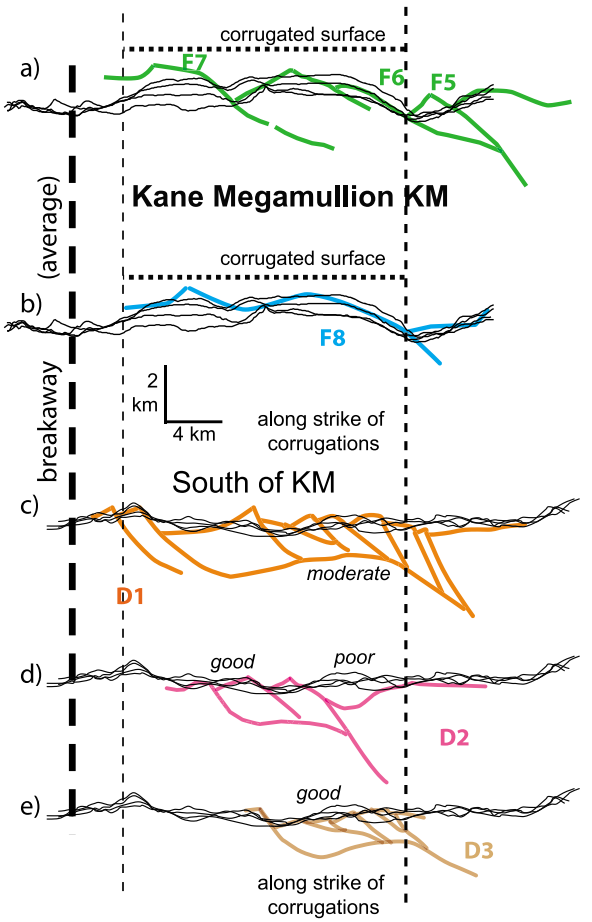

Figure 9. (a, b) Comparison between the bathymetry over the Kane Megamullion (for location of the bathymetric profiles see Figure 1) with the basement topography of the F6, F7, and F8 detachments. Although the Kane Megamullion is of greater flow line extent than F6, F7, or even F8, these match the dip of the ridgeward facing slope of the corrugated surface as well as the height of the Megamullion above its hanging wall cutoff. (c, d, e) The subdued seafloor topography to the south of the Kane Megamullion is compared with the basement topography above the D detachments. See text for discussion.

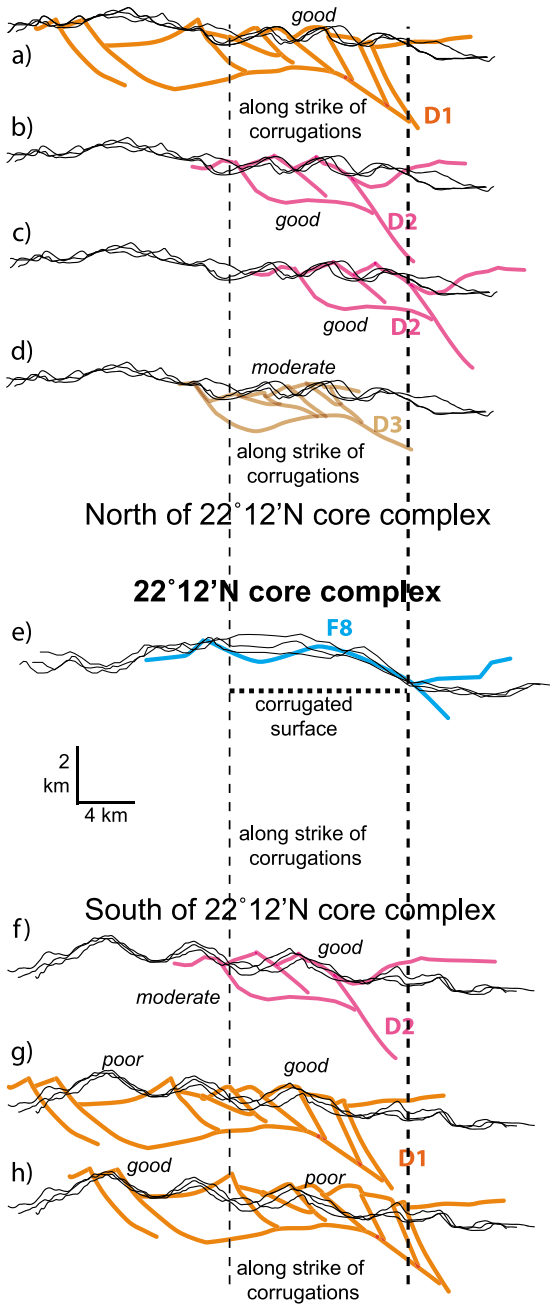

Figure 10. Comparison between the bathymetry over the 22°12′N OCC (e) with F8 and (a, b, c, d, f, g, h) between the bathymetry along strike of the OCC with the D detachments. The match is sufficient to suggest that F8 defines an OCC similar to that at 22°12′N and that detachment faults may occur beneath fault blocks along strike of OCCs. See text for discussion.

[24] Similarly, we compare the seafloor morphology along strike of the 22°12′N OCC (Figures 10a, 10b, and 10c) with that above the D1, D2 and D3 detachments. To the north of the OCC, the spacing of the fault blocks resembles that above the D2 detachment in particular (Figures 10 b and 10c). Although these fault blocks are larger that those above D3, the geometry of the breakaway and overall dimensions of the system are similar (Figure 10d). To the south of the 22°12′N OCC (Figures 10f, 10g, and 10h) the morphology of the basement top is rougher than that observed above either D1 or D2, but some resemblance can still be noticed, for instance in the frontal slope of the fault block above the D2 and D1 root zones (Figures 10f and 10g), the height and the tilt of the fault blocks (e.g., Figure 10f and the western end of Figure 10h) if not always their spacing.

[25] These comparisons highlight that the basement topography above the D detachments is as variable as that along strike of known OCCs. The comparison by no means proves that the OCC detachments continue as D style in the subsurface, but do add credence to the suggestion that they might. D-style

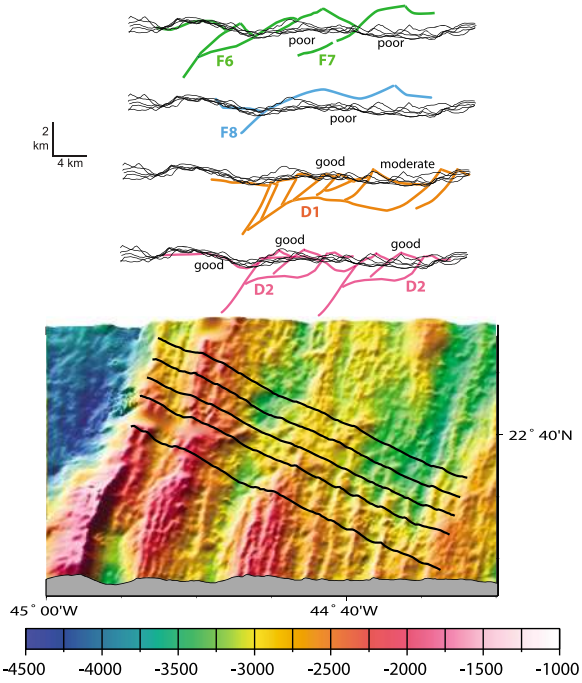

Figure 11. Comparison between the bathymetry away from modern OCCs and the topography and fault geometry above subsurface detachments imaged in seismic from the Canary Basin and Cape Verde Abyssal Plain. There is a reasonable match between this bathymetry and the basement topography along BIRPS OCEAN profiles 5 and 7, but not with the basement topography on Canary profile C. The comparison does not preclude the possibility that detachments may occur within the subsurface away from OCCs and thus may be more widespread in slow spreading crust than currently thought.

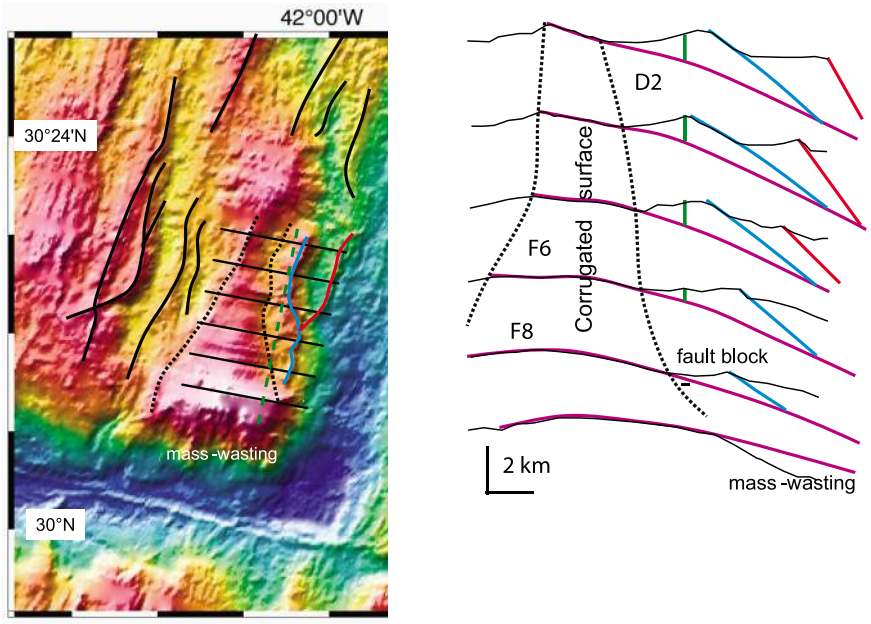

Figure 12. (left) Bathymetry of the Atlantis Massif, showing a corrugated surface narrowing to the north as the width of the rider block or rider blocks increases in the same direction. (right) Bathymetric profiles across this structure, showing interpretation in which the slip surface continues beneath these fault blocks to the north; the fault blocks represent successive slices of the hanging wall (blue then red) sliced off the hanging wall in a rolling hinge model. The depth to the detachment (indicated by green bars on the right) is constrained by seismic profile Meg-5 [*Canales et al.*, 2004], marked by a green line on the map.

detachments may thus be present beneath the small-scale tilted blocks that typically have been interpreted as a change in dominant fault style along strike of OCCs.

[26] Of course if OCCs are places where a D-style detachment breaks the surface, similar D-style detachments may exist where no OCC is observed along strike simply because that detachment system has nowhere broken the surface. A comparison (Figure 11) between the basement morphology of the F detachments shows that the subdued bathymetry away from OCCs does not match the topography of the F detachments but matches the basement topography above the D detachments reasonably well. This implies that detachments such as D1–D3 may exist beneath much of the crust formed at slow spreading rate. However, it should be emphasized that although the bathymetric data do not preclude such a possibility, neither do they strongly support it.

[27] The suggestion that a top of basement fault such as the F detachments may continue laterally beneath small fault blocks toward the center of a segment is supported by the structure of the Atlantis Massif just north of the Atlantis transform (Figure 12). Toward the inside corner (before reaching a portion of the Massif affected by slope failure), the corrugated surface is exposed and can be traced almost into the median valley. However, moving away from the transform, the fault disappears beneath a "slipped block" [*Cann et al.*, 1997] well before the edge of the median valley. The continuation of the main fault beneath the "slipped block" has been demonstrated by seismic reflection images [*Canales et al.*, 2004]. However, we propose that the "slipped block" has not slipped, but rather is a slice of the hanging wall transferred to and rafted with the footwall [*Ranero and Reston*, 1999; *Reston and Ranero*, 2005; *Smith et al.*, 2006; *Smith et al.*, 2008] by the development of a new fault propagating up from depth in a rolling hinge model [*Buck*, 1988] (see below). Further north, the bathymetric data (Figure 12) show that the rider block (or blocks) widen northward toward the segment middle, consistent with a northward deepening of the detachment.

[28] In summary, it appears possible that the corrugated slip surface of an OCC continues toward the middle of the segment beneath a series of small fault blocks. A remaining question is how such

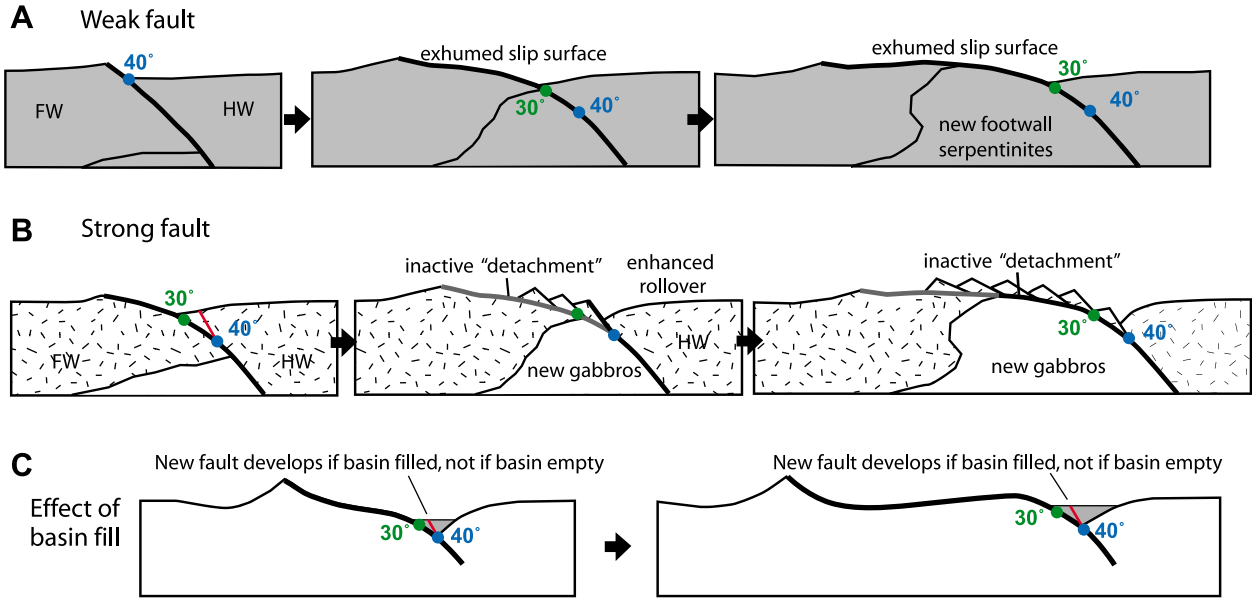

Figure 13. Rolling hinge models for the formation of detachment faults. (a) Simple model of a large offset weak fault [*Lavier et al.*, 1999], the footwall flexing as it is unloaded. Points where the modeled fault reaches dips of 30° and 40° are marked. As long as the fault is not rotated to an angle at which it should lock up while in the basement, a large expanse of the footwall may be exhumed to form the top of basement. In this model, the locking angle must be <30° as the fault remains active below this angle, meaning that the model applies only if fault strength is dominated by serpentinites, talc or other weak minerals. As a result, the model is labeled "weak fault." Such "top basement faults" form the corrugated surface of OCCs. (b) As in Figure 13a except the dominance of strong fault rocks (perhaps where the country rock is dominated by gabbros and basalts) means the fault locks up at ~35°. Once the upper portion of the fault locks up, a new fault propagates up from the root zone of the earlier fault, transferring a slice of the hanging wall to the footwall [*Buck*, 1988]. Movement continues until the new fault also rotates to an angle at which it locks up, requiring a new fault to cut through the hanging wall, again transferring a slice of the hanging wall to the footwall. Continued movement results in a subhorizontal "detachment" never active at low angle, covered with fault blocks, formed as successive slices off the hanging wall [*Buck*, 1988]. Such covered detachments may lie along strike of corrugated surfaces, the only difference being whether or not slices of the hanging wall have been rafted with the detachment or not. (c) Influence of presence or absence of basin fill. The development of a deep hanging wall basin in the models of *Schouten et al.* [2010] means that the slip surface is already exhumed when rotated to a locking angle of ~35° unless the basin is filled by basalts and basaltic rubble, in which case the fault remains in the subsurface beyond its locking angle. Thus in a basalt-filled basin, more likely to be found toward the center of a segment, the fault locks up and a slice of basalt is transferred from the hanging wall to the footwall to be rafted up and out.

structures develop and why they should be exposed at segment ends and buried toward segment middles.

5. Discussion: Rolling Hinge "Detachments"

[29] "Detachment faults" at segment middles have been interpreted [*Reston et al.*, 1996] as successive sections of a series of flexed normal faults in a rolling hinge model [*Buck*, 1988] rooting beneath the median valley at 30–40°. The geometry of the corrugated surface at segment ends [*Tucholke et al.*, 1998; *Reston et al.*, 2004a] is also consistent with a rolling hinge model: the flexural rotation of a single fault rooting beneath the median valley and active at 30–40° [*Lavier et al.*, 1999; *Tucholke et al.*, 2008] or at ~60° [*Schouten et al.*, 2010] (Figure 13).

[30] The fundamental difference between the rolling hinge models described by *Buck* [1988] and those described subsequently by others [*Lavier et al.*, 1999; *Buck et al.*, 2005; *Tucholke et al.*, 2008; *Schouten et al.*, 2010] is whether or not the flexure of the footwall rotates the fault beneath the seafloor to angles too low to be active (Figure 13). This is a function of the angle to which the fault is rotated, and how weak the fault is. If the shallow portion of the fault locks up in the subsurface but the steeper root zone remains active, new faults propagate up from the root zone through the hanging wall, transferring slices of the hanging wall to the foot-

wall [*Buck*, 1988]. These fault slices are then rafted upwards and outwards with the original footwall and as the underlying inactive fault segments are passively rotated to low angle, form a layer of fault blocks on top. The first step in this process has already been discussed with reference to the F6 and F5 detachments (Figure 7). However, if the fault is not rotated sufficiently to lock up in the subsurface, continued slip on the same surface results in the exhumation of a large expanse of the corrugated slip surface marking the top of the footwall. Thus whether an OCC develops or whether a detachment fault is covered by a layer of rafted blocks, in turn depends on whether the angle to which the normal fault can remain active (the "locking angle") is reached above or below the top hanging wall cutoff.

[31] From classical Mohr-Coulomb considerations, normal faults should be able to remain active at angles as low as perhaps 35° (Figure 13b), although this can be lower if the stress field is rotated, or if either high fluid pressures or a weak gouge develops along the faults (Figure 13a). Of these effects, a weak fault gouge is particularly likely to develop near inside corners where talc and serpentinites have been found [*Cannat*, 1996; *Reston et al.*, 2002, *Dannowski et al.*, 2010]: even partly serpentinised peridotites have an internal coefficient of friction of about 0.4 and talc is even weaker, allowing normal faults to remain active to perhaps 20–25° [*Escartín et al.*, 1997]. A weak gouge may develop not only if weak rocks form the bulk wall rock if for instance the shear zone wraps around a gabbro body [*Ildefonse et al.*, 2007], but also if the fault intersects even relatively minor proportions of peridotites: the volume increase during serpentinisation may force the serpentinites into the fault zone to be smeared along the fault by movement and perhaps even to be injected laterally along the fault as a slurry [*Dick et al.*, 2008]. The mobility of serpentine muds has been observed in the Marianas [*Fryer et al.*, 1999] and inferred at rifted margins [*Reston et al.*, 2004b].

[32] The increasing number of observations or interpretations of gabbros within OCCs [*Dick et al.*, 2000; *Reston et al.*, 2002; *Ildefonse et al.*, 2007; *Canales et al.*, 2008; *Planert et al.*, 2010] does not imply that the magmatic crust at segment ends is thicker than previously supposed, but may rather indicate that the detachment system tends to transfer the bulk of the oceanic lower crust to the footwall and the overlying basalts and dikes to the hanging wall, providing strongly asymmetric accretion [*Tucholke and Lin*, 1994; *Escartín et al.*, 2008; *Planert et al.*, 2010]. Total magmatic crust at segment middles remains thicker than that at segment ends, as shown by numerous studies of crustal structure [e.g., *Canales et al.*, 2000; *Planert et al.*, 2009].

[33] The numerical models discussed above show that as the footwall begins to flex, the hanging wall is deformed to form a basin against the footwall (Figure 13c). If this basin remains empty, much of the flexure and rotation of the footwall occurs in the portion of the footwall that has been exposed, whereas if the basin is filled by new extrusives, basaltic crust is juxtaposed against the flexed and rotating footwall, potentially burying the point at which the fault reaches the locking angle. As magmatism increases, as might be expected toward the center of a segment, it will be more likely that the fault will reach the locking angle in the subsurface and be abandoned. The fault propagating up to the surface from the still active root zone will then transfer a slice of new magmatic basin fill (lava flows, pillow lavas, basaltic rubble) to the hanging wall to be rafted up and out of the basin with the footwall. The section incorporated into these fault blocks will thus depend on the depth where the new faults splay off the root zone and on the stratigraphy of the oceanic crust, but as the fault blocks taper downward, deeper portions of the magmatic crust such as sheeted dikes and gabbros are likely to be volumetrically underrepresented.

[34] Changing the basin fill from water to basalt also changes the density contrast between the basin fill and the asthenosphere, and thus affects the flexural parameter, the control on the wavelength and amplitude of the flexure [*Turcotte and Schubert*, 2002]. The flexural parameter is however mainly controlled by the elastic thickness of the plate. As the flexural parameter controls the geometry of the flexure, it also influences the location of the locking angle: the thicker lithosphere at the colder segment end is likely to rotate less rapidly than the thinner lithosphere toward the warmer segment middle, further increasing the likelihood that the fault partially covered with lavas will lock up in the subsurface in the middle of a segment before so doing toward the end (Figures 13 and 14).

[35] All these variables predict the same tendency: the locking angle is more likely to occur within the subsurface near the middle of a segment than at a segment end, so that a detachment system may switch from an OCC topped by a corrugated surface at a segment end, representing the exhumed footwall of a single large-offset fault, to a system where the "detachment" was active as a series of

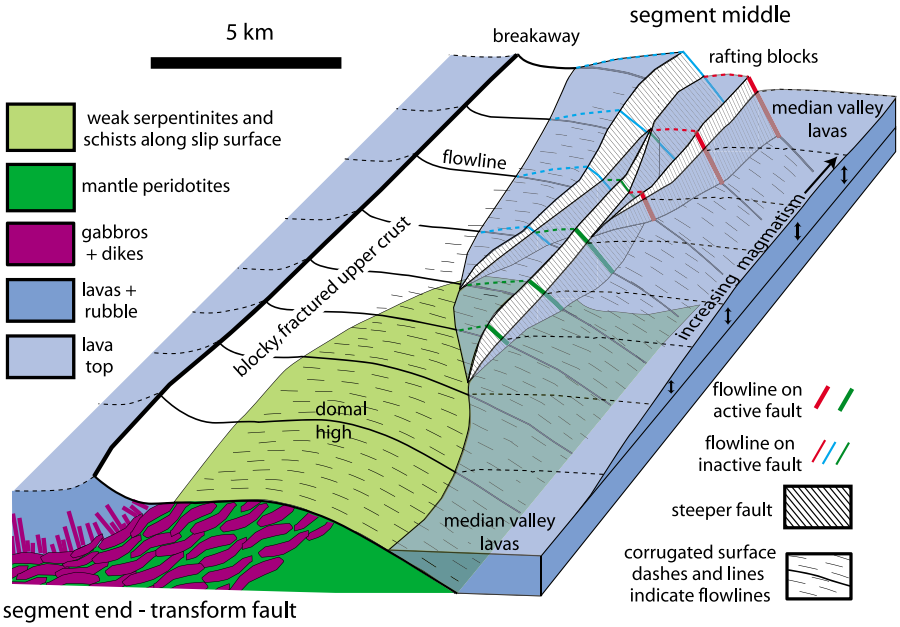

Figure 14. Perspective view of one side of a slow spreading ridge segment, showing a lateral transition from the unroofed footwall of a detachment at the segment end (modified after *Reston et al.* [2002] following discussions at the Chapman conference in Cyprus, May 2010) to a detachment buried beneath a series of rafted blocks toward the segment middle. The detachment is continuous along strike, but deepens beneath rafted blocks toward the segment center. The formation of the rafted blocks moving toward the segment middle is controlled by the migration into the subsurface of the point where fault locks up. This deepening of the locking point results from increasing magmatism partially burying the fault, disappearance of weak serpentinites as magmatic crust becomes dominant and laterally decreasing elastic thickness moving away from the segment end.

fault segments and overlain by a series of fault blocks. Thus not only is it possible that a detachment system continues laterally away from the corrugated surface beneath small fault blocks, but the change from an exhumed corrugated surface to a detachment system covered by rafted blocks is in keeping with thinner lithosphere, increased magmatism and reduced amounts of serpentinites toward the segment middle or at least toward a magmatic center (Figure 14).

6. Conclusions

[36] The seismic depth images discussed in this paper show two styles of "detachment fault" that together may form a single fault system at the spreading center. The first detachment fault style is a large-offset normal fault where the footwall to the fault has been exhumed as a convex-up basement high, forming an oceanic core complex (OCC). The second detachment fault style has similar dimensions, but the detachment is covered by a series of comparatively small fault blocks. We propose that both types of detachment faults are likely to originate through a rolling hinge mechanism, caused by the flexure of the footwall during unloading. The key difference is whether the fault locks up at relatively high angle in the subsurface or not: if the fault does lock up, a new fault propagating from depth transfers a slice of the hanging wall to the footwall, the slice subsequently being rafted out of the median valley with the exhuming footwall; repetition produces an inactive "detachment" covered by a series of rafted fault slices.

[37] The switch from a nonlocking to locking fault is likely to be controlled by a combination of changing fault properties, especially the presence of low friction talc and serpentinites along the fault, laterally variable elastic thickness and changes in the amount of lavas filling in the basin adjacent to the fault. As all of these factors mean that faults are most likely to lock up within the subsurface at relatively high angles toward the middle of a segment (less talc and serpentine, weaker and more tightly flexed lithosphere, thicker sequences of lavas abutting the exhuming footwall). Thus toward the middle of segments, detachment faults may be present beneath a series of small fault blocks, whereas at segment ends, the detachment does not lock up in the subsurface, so that continued slip

even at low angles results in the exhumation of the footwall slip surface to form an OCC.

[38] The implication is that detachment faults may be present even where no corrugated surfaces are imaged with seafloor mapping techniques and where the seafloor topography is dominated by small tilted fault blocks. Detachment faulting may be more widespread at slow spreading ridges than generally interpreted from seafloor studies alone. However, whether detachments extend for whole segments or are laterally replaced by increased magmatism remains to be investigated.

Acknowledgments

[39] We are grateful to Roger Buck and Brian Tucholke for thorough and thoughtful reviews. The depth images were generated at IFM-GEOMAR and at ICREA using the Omega2 software (Western-Geco) and its forerunners SEISMOS and GEOSYS, prestack depth migration software SIRIUS and its predecessor Migpack from GXT, and GMT. Reston acknowledges past support from the Deutsche Forschungsgemeinschaft through grants Re 873/ 11 and 12. Reston also acknowledges the contribution of participants at the Oceanic Detachment Faulting meeting held in Cyprus in May 2010.

References

Blackman, D. K., J. R. Cann, B. Janssen, and D. K. Smith (1998), Origin of extensional core complexes: Evidence from the Mid-Atlantic Ridge at Atlantis Fracture Zone, *J. Geophys. Res.*, *103*, 21,315–21,333, doi:10.1029/98JB01756.

Blackman, D. K., J. P. Canales, and A. Harding (2009), Geophysical signatures of oceanic core complexes, *Geophys. J. Int.*, *178*, 593–613, doi:10.1111/j.1365-246X.2009.04184.x.

Buck, W. R. (1988), Flexural rotation of normal faults, *Tectonics*, *7*, 959–973, doi:10.1029/TC007i005p00959.

Buck, W. R., L. L. Lavier, and A. N. B. Poliakov (2005), Modes of faulting at mid-ocean ridges, *Nature*, *434*, 719–723, doi:10.1038/nature03358.

Canales, J. P., R. S. Detrick, J. Lin, J. A. Collins, and D. R. Toomey (2000), Crustal and upper mantle seismic structure beneath the rift mountains and across a nontransform offset at the Mid-Atlantic Ridge (35°N), *J. Geophys. Res.*, *105*(B2), 2699–2719, doi:10.1029/1999JB900379.

Canales, J. P., B. E. Tucholke, and J. A. Collins (2004), Seismic reflection imaging of an oceanic detachment fault: Atlantis megamullion (Mid-Atlantic Ridge, 30°10′N), *Earth Planet. Sci. Lett.*, *222*, 543–560, doi:10.1016/j.epsl.2004.02.023.

Canales, J. P., B. E. Tucholke, M. Xu, J. A. Collins, and D. L. DuBois (2008), Seismic evidence for large-scale compositional heterogeneity of oceanic core complexes, *Geochem. Geophys. Geosyst.*, *9*, Q08002, doi:10.1029/2008GC002009.

Cann, J. R., D. K. Blackman, D. K. Smith, E. McAllister, B. Janssen, S. Mello, E. Avgerinos, A. R. Pascoe, and J. Escartín (1997), Corrugated slip surfaces formed at ridge-transform intersections on the Mid-Atlantic Ridge, *Nature*, *385*, 329–332, doi:10.1038/385329a0.

Cannat, M. (1996), How thick is the magmatic crust at slow spreading ridges?, *J. Geophys. Res.*, *101*, 2847–2857, doi:10.1029/95JB03116.

Dannowski, A., I. Grevemeyer, C. R. Ranero, G. Ceuleneer, M. Maia, J. P. Morgan, and P. Gente (2010), Seismic structure of an oceanic core complex at the Mid-Atlantic Ridge, 22°19′N, *J. Geophys. Res.*, *115*, B07106, doi:10.1029/2009JB006943.

deMartin, B., R. A. Sohn, J. P. Canales, and S. E. Humphris (2007), Kinematics and geometry of active detachment faulting beneath the Trans-Atlantic Geotraverse (TAG) hydrothermal field on the Mid-Atlantic Ridge, *Geology*, *35*, 711–714, doi:10.1130/G23718A.1.

Dick, H. J. B., et al. (2000), A long in situ section of the lower ocean crust: Results of ODP Leg 176 drilling at the Southwest Indian Ridge, *Earth Planet. Sci. Lett.*, *179*, 31–51, doi:10.1016/S0012-821X(00)00102-3.

Dick, H. J. B., M. A. Tivey and B. E. Tucholke (2008), Plutonic foundation of a slow spreading ridge segment: Oceanic core complex at Kane Megamullion, 23°30′N, 45°20′W, *Geochem. Geophys. Geosyst.*, *9*, Q05014, doi:10.1029/2007GC001645.

Escartín, J., G. Hirth, and B. Evans (1997), Effects of serpentinization on the lithospheric strength and the style of normal faulting at slow spreading ridges, *Earth Planet. Sci. Lett.*, *151*, 181–189, doi:10.1016/S0012-821X(97)81847-X.

Escartín, J., C. Mevel, C. J. MacLeod, and A. M. McCaig (2003), Constraints on deformation conditions and the origin of oceanic detachments: The Mid-Atlantic Ridge core complex at 15°45′N, *Geochem. Geophys. Geosyst.*, *4*(8), 1067, doi:10.1029/2002GC000472.

Escartín, J., D. K. Smith, J. Cann, H. Schouten, C. H. Langmuir, and S. Escrig (2008), Central role of detachment faults in accretion of slow spreading oceanic lithosphere, *Nature*, *455*, 790–794, doi:10.1038/nature07333.

Fryer, P., C. G. Wheat, and M. Mottl (1999), Mariana blueschist mud volcanism: Implications for conditions within the subduction zone, *Geology*, *27*, 103–106, doi:10.1130/0091-7613(1999)027<0103:MBMVIF>2.3.CO;2.

Garcés, M., and J. Gee (2007), Paleomagnetic evidence of large footwall rotation associated with low-angle faults at the Mid-Atlantic Ridge, *Geology*, *35*, 279–282, doi:10.1130/G23165A.1.

Ildefonse, B., D. K. Blackman, B. E. John, Y. Ohara, D. J. Miller, C. J. MacLeod, and the Integrated Ocean Drilling Program Expeditions 304–305 Science Party (2007), Oceanic core complexes and crustal accretion at slow spreading ridges, *Geology*, *35*, 623–626, doi:10.1130/G23531A.1.

Lavier, L. L., W. R. Buck, and A. N. B. Poliakov (1999), Self-consistent rolling-hinge model for the evolution of large-offset low-angle normal faults, *Geology*, *27*, 1127–1130, doi:10.1130/0091-7613(1999)027<1127:SCRHMF>2.3.CO;2.

MacLeod, C. J., et al. (2002), Direct geological evidence for oceanic detachment faulting; the Mid-Atlantic Ridge, 15 degrees 45′N, *Geology*, *30*, 879–882, doi:10.1130/0091-7613(2002)030<0879:DGEFOD>2.0.CO;2.

MacLeod, C. J., R. C. Searle, B. J. Murton, J. F. Casey, C. Mallows, S. C. Unsworth, K. L. Achenbach, and M. Harris (2009), Life cycle of oceanic core complexes, *Earth Planet. Sci. Lett.*, *287*, 333–344, doi:10.1016/j.epsl.2009.08.016.

Morris, A., J. S. Gee, N. Pressling, B. E. John, C. J. MacLeod, C. B. Grimes, and R. C. Searle (2009), Footwall rotation in an oceanic core complex quantified using reoriented Integrated

Ocean Drilling Program core samples, *Earth Planet. Sci. Lett.*, *287*, 217–228, doi:10.1016/j.epsl.2009.08.007.

Olive, J.-A., M. D. Behn, and B. E. Tucholke (2010), The structure of oceanic core complexes controlled by the depth distribution of magma emplacement, *Nat. Geosci.*, *3*, 491–495, doi:10.1038/ngeo888.

Planert, L., E. Flueh, and T. J. Reston (2009), Along and across-axis variations in crustal thickness and structure at the Mid-Atlantic Ridge at 5° South obtained from wide-angle seismic tomography: Implications for ridge-segmentation, *J. Geophys. Res.*, *114*, B09102, doi:10.1029/2008JB006103.

Planert, L., E. R. Flueh, F. Tilmann, I. Grevemeyer, and T. Reston (2010), Crustal structure of a rifted oceanic core complex and its conjugate side at the MAR at 5°S: Implications for melt extraction during detachment faulting and core complex formation, *Geophys. J. Int.*, *181*, 113–126, doi:10.1111/j.1365-246X.2010.04504.x.

Ranero, C. R., and T. J. Reston (1999), Detachment faulting at ocean core complexes, *Geology*, *27*, 983–986, doi:10.1130/0091-7613(1999)027<0983:DFAOCC>2.3.CO;2.

Ranero, C. R., E. Banda, and P. Buhl (1997a), The crustal structure of the Canary Basin: Accretion processes at slow spreading centers, *J. Geophys. Res.*, *102*, 10,185–10,201, doi:10.1029/97JB00101.

Ranero, C. R., T. J. Reston, I. Belykh, and H. Gnibidenko (1997b), Reflective oceanic crust formed at a fast-spreading center in the Pacific, *Geology*, *25*, 499–502, doi:10.1130/0091-7613(1997)025<0499:ROCFAA>2.3.CO;2.

Reston, T. J. (1996), The S reflector west of Galicia: The seismic signature of a detachment fault, *Geophys. J. Int.*, *127*, 230–244, doi:10.1111/j.1365-246X.1996.tb01547.x.

Reston, T. J., and C. R. Ranero (2005), Detachment faulting within slow spreading segments: Beyond the corrugated surface, *Eos Trans. AGU*, *86*(52), Fall Meet. Suppl., Abstract T34B-05.

Reston, T. J., O. Ruoff, J. H. McBride, C. R. Ranero, and R. S. White (1996), Detachment and steep faulting in the oceanic crust west of Africa, *Geology*, *24*, 811–814, doi:10.1130/0091-7613(1996)024<0811:DASNFI>2.3.CO;2.

Reston, T. J., W. Weinrebe, I. Grevemeyer, E. R. Flueh, N. C. Mitchell, L. Kirstein, C. Kopp, H. Kopp, and participants of Meteor 47/2 (2002), A rifted inside corner massif on the Mid-Atlantic Ridge at 5°S, *Earth Planet. Sci. Lett.*, *200*, 255–269, doi:10.1016/S0012-821X(02)00636-2.

Reston, T. J., C. R. Ranero, O. Ruoff, M. Perez-Gussinye, and J. J. Danobeitia (2004a), Geometry of extensional faults developed at slow spreading centres from seismic reflection data in the Central Atlantic (Canary Basin), *Geophys. J. Int.*, *159*, 591–606.

Reston, T. J., V. Gaw, J. Pennell, D. Klaeschen, A. Stubenrauch, and I. Walker (2004b), Extreme crustal thinning in the south Porcupine Basin and the nature of the Porcupine Median High: Implications for the formation of non-volcanic rifted margins, *J. Geol. Soc.*, *161*, 783–798, doi:10.1144/0016-764903-036.

Schouten, H., D. K. Smith, J. R. Cann, and J. Escartín (2010), Tectonic versus magmatic extension in the presence of core complexes at slow spreading ridges from a visualization of faulted seafloor topography, *Geology*, *38*, 615–618, doi:10.1130/G30803.1.

Shaw, P. R., and J. Lin (1993), Causes and consequences of variations in faulting style at the Mid-Atlantic Ridge, *J. Geophys. Res.*, *98*, 21,839–21,851, doi:10.1029/93JB01565.

Singh, S., W. Crawford, H. Carton, T. Seher, V. Combier, M. Cannat, J. Canales, D. Düsünür, J. Escartín, and J. Miranda (2006), Discovery of a magma chamber and faults beneath a Mid-Atlantic Ridge hydrothermal field, *Nature*, *442*, 1029–1032, doi:10.1038/nature05105.

Smith, W. H. F., and D. T. Sandwell (1995), Marine gravity field from declassified Geosat and ERS-1 altimetry, *Eos Trans. AGU*, *76*(46), Fall Meet. Suppl., F156.

Smith, D. K., J. R. Cann, and J. Escartín (2006), Widespread active detachment faulting and core complex formation near 13°N on the Mid-Atlantic Ridge, *Nature*, *442*, 440–443, doi:10.1038/nature04950.

Smith, D. K., J. Escartin, H. Schouten, and J. Cann (2008), Fault rotation and core complex formation: Significant processes in seafloor formation at slow spreading mid-ocean ridges (Mid-Atlantic Ridge, 13°–15°N), *Geochem. Geophys. Geosyst.*, *9*, Q03003, doi:10.1029/2007GC001699.

Tucholke, B. E., and J. Lin (1994), A geological model for the structure of ridge segment in slow spreading ocean crust, *J. Geophys. Res.*, *99*, 11,937–11,958, doi:10.1029/94JB00338.

Tucholke, B. E., J. Lin, and M. C. Kleinrock (1998), Megamullions and mullion structure defining oceanic metamorphic core complexes on the Mid-Atlantic Ridge, *J. Geophys. Res.*, *103*, 9857–9866, doi:10.1029/98JB00167.

Tucholke, B. E., M. D. Behn, W. R. Buck, and J. Lin (2008), Role of melt supply in oceanic detachment faulting and formation of megamullions, *Geology*, *36*, 455–458, doi:10.1130/G24639A.1.

Turcotte, D. L., and G. Schubert (2002), *Geodynamics*, 456 pp., Cambridge Univ. Press, Cambridge, UK.

White, R. S., J. H. McBride, T. J. Henstock, and R. W. Hobbs (1994), Internal structure of Mesozoic oceanic crust, *Geology*, *22*, 597–600, doi:10.1130/0091-7613(1994)022<0597:ISOASS>2.3.CO;2.